In vivo detection of epileptic brain tissue using static fluorescence and diffuse reflectance spectroscopy

Nitin Yadav
Sanjiv Bhatia
John Ragheb
Rupal Mehta
Prasanna Jayakar
William Yong
Wei-Chiang Lin

In vivo detection of epileptic brain tissue using static fluorescence and diffuse reflectance spectroscopy

Nitin Yadav,[a] **Sanjiv Bhatia,**[b] **John Ragheb,**[b] **Rupal Mehta,**[c] **Prasanna Jayakar,**[b] **William Yong,**[c] **and Wei-Chiang Lin**[a,b]
[a]Florida International University, Department of Biomedical Engineering, Miami, Florida
[b]The Brain Institute, Miami Children's Hospital, Miami, Florida
[c]University of California at Los Angeles, Department of Pathology, Los Angeles, California

Abstract. Diffuse reflectance and fluorescence spectroscopy are used to detect histopathological abnormalities of an epileptic brain in a human subject study. Static diffuse reflectance and fluorescence spectra are acquired from normal and epileptic brain areas, defined by electrocorticography (ECoG), from pediatric patients undergoing epilepsy surgery. Biopsy specimens are taken from the investigated sites within an abnormal brain. Spectral analysis reveals significant differences in diffuse reflectance spectra and the ratio of fluorescence and diffuse reflectance spectra from normal and epileptic brain areas defined by ECoG and histology. Using these spectral differences, tissue classification models with accuracy above 80% are developed based on linear discriminant analysis. The differences between the diffuse reflectance spectra from the normal and epileptic brain areas observed in this study are attributed to alterations in the static hemodynamic characteristics of an epileptic brain, suggesting a unique association between the histopathological and the hemodynamic abnormalities in an epileptic brain.
© *2013 Society of Photo-Optical Instrumentation Engineers (SPIE)* [DOI: 10.1117/1.JBO.18.2.027006]

Keywords: diffuse reflectance spectroscopy; fluorescence spectroscopy; brain surgery; pediatric epilepsy.

Paper 12565R received Aug. 30, 2012; revised manuscript received Dec. 5, 2012; accepted for publication Jan. 17, 2013; published online Feb. 5, 2013.

1 Introduction

According to the Epilepsy Foundation, of the 200,000 new cases of epilepsy diagnosed each year in the United States, 45,000 are in children under the age of 15.[1] Epilepsy is considered a severe neurological disorder in children, because its primary symptom, seizure, can severely damage normal brain development. When pharmaceutical and/or dietary therapies fail to achieve seizure freedom, epilepsy is defined as refractory.[2,3] For pediatric patients with refractive epilepsy, surgical intervention, when applicable, becomes necessary. Since the success of epilepsy surgery is determined by the amount of seizure-inducing cortex (i.e., epileptic cortex) removed, there arises a need to develop some systematic methodology that accurately detects and demarcates the epileptic cortex pre- and intra-operatively.

Noninvasive diagnostic technologies commonly used in the presurgical planning of epilepsy surgery include electro-encephalography (EEG), video EEG, and several noninvasive imaging modalities like computed tomography (CT), single-photon emission computed tomography (SPECT), magnetic resonance imaging, positron emission tomography, and diffusion tensor imaging.[4–8] Advancements in noninvasive imaging modalities over the past two decades have greatly improved their ability to identify epileptic cortex or lesions and hence improve surgical outcomes.[4,7,8] However, the above mentioned diagnostic technologies, when used individually, cannot provide definitive information on which surgery can be based; at best, they provide approximate locations of seizure origins, due to their limited sensitivity and spatial resolution.[4,7,9] In addition, these technologies may be difficult to use on pediatric patients, who may not be able to remain motionless for extended periods.[10]

Finally, spatial coordinates of the epileptic cortex defined in these studies may lose their value because of brain shift/deformation during the craniotomy procedure.[11–14]

When EEG/imaging studies are inconclusive, electrocorticography (ECoG) may be used to perform invasive mapping of the ictal onset zone.[9,15] In addition, ECoG is used in the operating room to detect interictal epileptiform discharges directly from the abnormal brain region; these discharges are used to define the resection margins for the surgeon. However, ECoG may also detect interictal discharges in a normal brain, as a result of electrical spreading, and epileptic focus localization using interictal discharges is subject to a certain amount of uncertainty in an anesthetized brain.[15] Histological evaluation of the epileptic cortex has uncovered many unique pathological features, such as balloon cells and cortical dislamination.[16] This information usually is acquired through postoperational histopathological analysis of the resected brain specimens and is not immediately available in the operating room. While histopathological features of the lesion may not correlate with surgical outcomes,[7,17] it is not yet clear if their presence can be used as an objective indicator with which to demarcate the area of an epileptic brain. The technological shortcomings and limitations described above frequently lead to incomplete removal of epileptic lesions, which adversely affects surgical outcomes. This is especially true for cases of extra-temporal epilepsy, which is common in children.[4,8,10,17] For these reasons, new technologies for intraoperative identification and demarcation of the epileptic brain area are needed to enhance the prognosis of epilepsy surgery for patients with intractable nonlesional extra-temporal epilepsy. These new technologies, ideally, should be developed in accordance with the intrinsic characteristics of an epileptic brain during the interictal period.

Address all corresponding author: Wei-Chiang Lin, 10555 W. Flagler Street EAS 2673, Miami, FL 33174. Tel: +305-348-6112; Fax: +305-348-6954; E-mail: wclin@fiu.edu

Because the intrinsic compositional and structural characteristics of tissue strongly affect its absorption and scattering properties, it is feasible to use the interaction between light and biological tissue to estimate these qualities and hence detect whatever alterations that result from disease development.[18–28] Such an optic-based diagnostic technology often is termed optical diagnosis; its advantages include its low cost, portability, and real-time application. Many of the existing optical diagnostic methodologies are based on fluorescence and diffuse reflectance spectroscopy. This is because several intrinsic biological chromophores (e.g., hemoglobin) and fluorophores (e.g., NADH) can be used to assess critical intrinsic physiological characteristics of biological tissue, including its hemodynamics and metabolism.[26,27,29–31] The feasibility of using optical spectroscopy to guide cancer surgery intra-operatively has been evaluated for various cancer types. Several studies have shown that combined fluorescence and/or diffuse reflectance spectroscopy can accurately detect brain tumors *in vivo* and hence may be used to guide brain tumor resection.[21,32] However, applying optical spectroscopy to the detection of the epileptic cortex has been explored in only a limited fashion to date.[33–37]

In this paper, combined fluorescence and diffuse reflectance spectroscopy is used to detect unique pathophysiological and morphological characteristics of the epileptic cortex in an *in vivo* human study. Static diffuse reflectance and fluorescence spectra are acquired from *in vivo* epileptic and normal cortex of pediatric patients undergoing epilepsy surgery. Spectral data are analyzed using various statistical tools, and unique spectral features associated with epileptic brain tissue defined by histology and ECoG are identified. The physiological underlying mechanisms responsible for these spectral alterations are extrapolated.

2 Materials and Methods

2.1 Instrumentation

For this study, a portable spectroscopy system was used to acquire fluorescence and diffuse reflectance spectra from the brain. The system consists of two light sources: a pulsed nitrogen laser (VSL-337; Spectra Physics) for fluorescence spectroscopy and a portable halogen lamp (LS-1; Ocean Optics) for diffuse reflectance spectroscopy. Since data collection was performed in a sterile field, a sterilizable fiberoptic probe was used in conjunction with the spectroscopy system. The probe consisted of seven 300-micron core optical fibers, which were arranged in the typical six-around-one fashion. The center-to-center distance between two adjacent fibers was about 750 μm. Two of the surrounding optical fibers, one at 12 o'clock and the other at 6 o'clock, were used to conduct excitation light, and the remaining fibers were used for reflected light collection. Based on the arrangement of the optical fibers in the probe, its volume of investigation was estimated at roughly 1 mm^3. The collection fibers of the optical probe were connected to a spectrometer (USB 2000-FL Spectrometer; Ocean Optics) with a spectral range of approximately 300 to 900 nm. The spectrometer was connected to a computer via a universal serial interface. A computer program was developed using LabView from National Instruments to control the entire spectral acquisition procedure.

2.2 Study Procedure

Static fluorescence and diffuse reflectance spectra were acquired from normal and epileptic brain areas, as defined via preoperative imaging and ECoG studies, in pediatric patients undergoing epilepsy surgery. Five or more measurement sites were selected for each patient at the exposed brain surface by the surgeon. These sites usually were equally distributed within and outside the resection zone. Prior to the spectral acquisition procedure, the investigated site was cleansed using saline to remove residual blood on the surface. The optical probe was placed in direct contact with the cortical surface without deforming the brain surface, and three spectra (i.e., baseline, fluorescence, and diffuse reflectance spectra) were acquired sequentially. Spectral acquisition was repeated three times. This procedure took less than 15 s to complete. The locations of the optically investigated sites and their spatial correlation with the ECoG electrode grids were documented using a digital camera. Biopsies were taken from the investigated sites within the zone of resection and stored in a 10% buffered formalin solution for subsequent histological analysis.

2.3 Histological Evaluation

All specimens collected in this study were processed in a histology lab. They were embedded in paraffin wax and then sectioned. From each specimen, three or four sections with a thickness of 4 μm were cut and stained using the conventional hematoxylin and eosin staining method. The prepared sections were evaluated by a neuropathologist at the University of California, Los Angeles (Dr. Rupal Mehta). These tissue sections were assessed for architectural laminar disorder, cytomegaly, dysmorphism, and balloon cell change. These findings were graded from 0 to 3 (0 for none, 1 for mild, 2 for moderate, and 3 for severe). The presence of binucleated cells and calcification was noted separately. These morphological characteristics were used to categorize spectral data as either normal or histologically abnormal.

2.4 Data Processing

All spectral data acquired from the *in vivo* study were preprocessed to remove any artifacts induced by instrumentation. Mainly, baseline subtraction and calibration factor applications were performed to all acquired fluorescence spectra $F(\lambda)$ and diffuse reflectance spectra $Rd(\lambda)$. The calibration factors used here were derived from the ratio of true and measured emission spectra from a calibrated light source.[38] Furthermore, to speed up the data analysis procedure, spectral range and resolution were further reduced. Specifically, diffuse reflectance data between 400 and 850 nm and fluorescence data between 380 and 750 nm were preserved; spectral resolution was reduced to 5 nm. In addition to the individual spectral types, a combined spectrum was created for the data analysis process, specifically the ratio of the fluorescence and diffuse reflectance spectra [i.e., $F(\lambda)/Rd(\lambda)$]. The wavelength range of the combined spectra was 400 to 750 nm, and the resolution was 5 nm. Several normalization techniques were applied to the preprocessed spectra, including local maximum normalization, area-under-the-curve normalization, global mean normalization, and arbitrary reference normalization (Fig. 1). For local maximum normalization, each spectrum is normalized to its maximum value. That is, $S_{\max}(\lambda) = S(\lambda)/\text{MAX}[S(\lambda)]$, where $S(\lambda)$ represents either

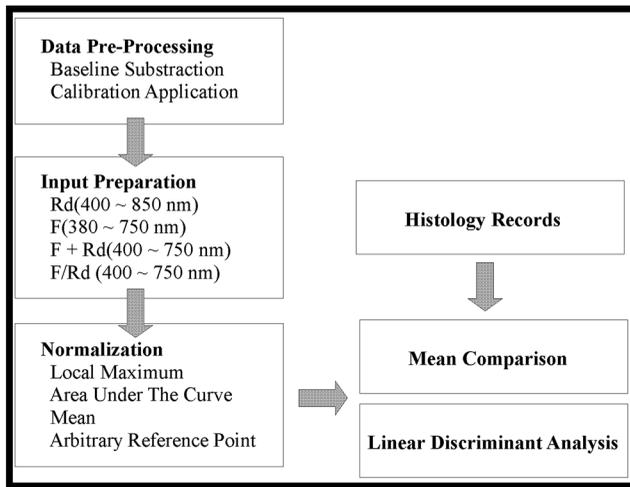**Data Pre-Processing**
Baseline Substraction
Calibration Application

↓

Input Preparation
Rd(400 ~ 850 nm)
F(380 ~ 750 nm)
F + Rd(400 ~ 750 nm)
F/Rd (400 ~ 750 nm)

↓

Normalization
Local Maximum
Area Under The Curve
Mean
Arbitrary Reference Point

Histology Records

↓

Mean Comparison

Linear Discriminant Analysis

Fig. 1 The flow chart of the data processing procedure employed in the study.

$F(\lambda)$, $Rd(\lambda)$, or $F(\lambda)/Rd(\lambda)$, and MAX is the maximum operation. For area-under-the-curve normalization, the new spectrum $S_{AREA}(\lambda)$ is calculated by $S_{AREA}(\lambda) = S(\lambda)/\int S(\lambda)d\lambda$. For global mean normalization, each spectrum is normalized to the mean of the total spectral data set. That is, $S_{MEAN}(\lambda) = S(\lambda)/[\sum_n S_i(\lambda)/n]$, where n represents the total number of spectra in the dataset. Finally, arbitrary reference normalization produces a new spectrum using $S_{POINT}(\lambda) = S(\lambda)/S(\lambda_{ref})$, where λ_{ref} is an arbitrary reference wavelength.

2.5 Data Analysis and Classification Algorithm Development

The main objective of this analysis was to determine if *in vivo* fluorescence and diffuse reflectance spectroscopy can detect histopathological and/or pathophysiological characteristics that are unique to epileptic brain tissue. To achieve this goal, the spectral data collected were classified using the results of histological analysis: the normal brain data containing spectral data measured from brain tissue outside the zone of resection, and the epileptic brain data containing spectral data from epileptic brain tissue confirmed by both histology and ECoG. To identify spectral regions and unique spectral features distinguishing epileptic brain tissue from the normal cortex, mean comparisons of the processed spectra from the two types of brain tissue (normal versus epileptic) were performed for all wavelengths. Depending on the distribution and variance characteristics of the data, either parametric (i.e., Student's *t*-test) or nonparametric tests (Wilcoxon Rank Sum test) were employed for mean comparisons. Next, tissue classification algorithms were developed based on linear discriminant analysis (LDA), for the purpose of determining the accuracy of using optical spectroscopy to differentiate between normal and epileptic brain tissue. LDA inputs were the spectral data from the normal and epileptic brain. Spectral data at all wavelengths were used in this process to create a model of discrimination, and standardized canonical coefficients were used to assess the importance of the spectral data region in determining tissue type. It was important to ensure that the discrimination model was statistically significant in terms of distinguishing a normal brain from an epileptic brain; therefore, only models associated with chi-square p values of less than 0.05 were considered. Furthermore, only models

with a sensitivity and specificity greater than 75% were considered successful and reported here. Finally, tissue type classification was validated using the leave-one-out method, and cross-validated sensitivity and specificity were reported.

3 Results

A total of 16 patients were enrolled in this study; their demographic information is summarized in Table 1. A total of 84 useful investigated sites were obtained from these patients: 28 located outside the resection zone defined by ECoG (i.e., normal brain) and 56 within the zone of resection. The 56 sites within the zone of resection were divided into two subcategories in accordance with the results of our histological evaluation; 30 sites exhibited histological features associated with epilepsy (epileptic brain), while the other 26 sites did not. The distribution of sites is shown in Table 2.

Spectral data analysis revealed that only those spectral differences identified within the original $Rd(\lambda)$, $Rd_{MEAN}(\lambda)$, $Rd_{POINT}(\lambda)$, and $F/Rd_{POINT}(\lambda)$ could produce discrimination

Table 1 Demographic information of the patients studied.

Patient number	Patient age/gender
1	3/M
2	4/F
3	4/M
4	6/M
5	2/F
6	14/F
7	8/F
8	21/F
9	2/M
10	20/F
11	17/F
12	5/M
13	3/F
14	16/F
15	10/M
16	3/M

Table 2 Distribution of the investigated sites.

ECoG	Pathology	Site #
–	NA	28
+	–	26
+	+	30

algorithms with a sensitivity and specificity greater than 75%. Analytical results for each spectral type follow.

3.1 Original $Rd(\lambda)$

Comparing the original $Rd(\lambda)$ from normal and epileptic brains revealed significantly different mean $Rd(\lambda)$ intensities between 400 and 600 nm ($p < 0.05$, see Fig. 2). Inputting the Rd signals from this spectral band, the best classification result based on LDA was 82.1% sensitivity, 76.7% specificity, and 79.3% total accuracy.

3.2 $Rd_{MEAN}(\lambda)$

Similar to original $Rd(\lambda)$, $Rd_{MEAN}(\lambda)$ between 400 and 600 nm also was statistically different between normal and epileptic brains ($p < 0.05$, see Fig. 3). Entering the signals from this spectral band, the best classification result based on LDA was 75.0%
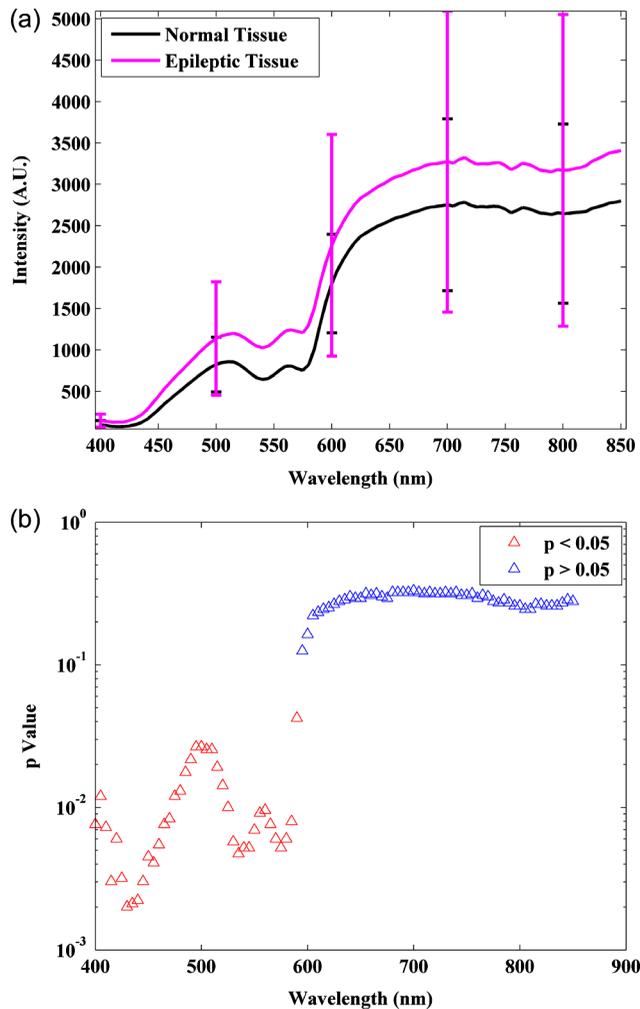
sensitivity, 83.3% specificity, and 79.3% overall accuracy, which is comparable to using the original $Rd(\lambda)$.

3.3 $Rd(\lambda)/Rd(\lambda_{ref})$

Analyzing $Rd(\lambda)/Rd(\lambda_{ref})$, as shown in Fig. 4, revealed several spectral features that could effectively differentiate a normal brain from an epileptic brain. Most of these spectral features were evident between $\lambda_{ref} = 400$ and $\lambda_{ref} = 600$ nm. Entering these identified spectral features, classification results based on LDA were ~75% sensitivity and ~80% specificity (Table 3). Discrimination was optimized when λ_{ref} was 505 nm, where the overall accuracy of the discrimination algorithm was 86.2%.

3.4 $[F(\lambda)/Rd(\lambda)]/[F(\lambda_{ref})/Rd(\lambda_{ref})]$

Analysis of $[F(\lambda)/Rd(\lambda)]/[F(\lambda_{ref})/Rd(\lambda_{ref})]$, as shown in Fig. 5, also revealed several spectral features from the combined spectrum that could effectively distinguish a normal brain from
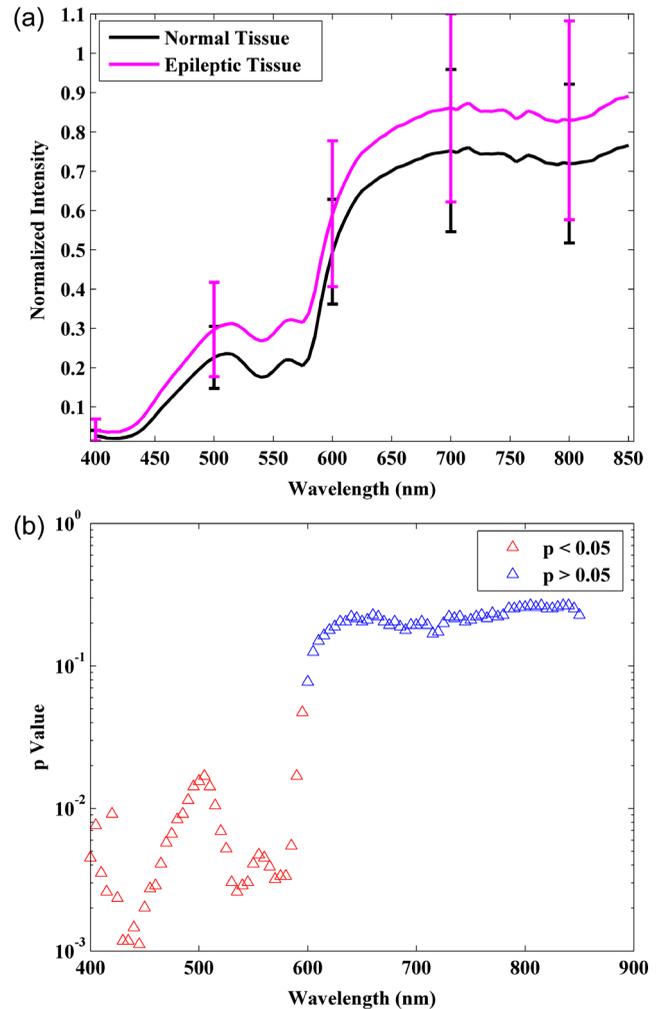

Fig. 2 (a) The solid black line represents the mean original $Rd(\lambda)$ from the normal brain group, and the solid pink line represents the mean original $Rd(\lambda)$ from the epileptic brain group. The error bars represent one standard deviation of the mean. (b) Statistical mean comparison of original $Rd(\lambda)$ between normal and epileptic brains; p value is below 0.05 between 400 and 600 nm. The optimal performance of the classification based on LDA, using original $Rd(\lambda)$ as the inputs, was sensitivity = 82.1%, specificity = 76.7%, and total correct classification = 79.3%.

Fig. 3 (a) The solid black line represents the mean $Rd_{MEAN}(\lambda)$ from the normal brain group, and the solid pink line represents the mean $Rd_{MEAN}(\lambda)$ from the epileptic brain group. The error bars represent one standard deviation of the mean. (b) Statistical mean comparison of $Rd_{MEAN}(\lambda)$ between normal and epileptic brains; p value is below 0.05 between 400 and 600 nm. The optimal performance of the classification based on LDA, using $Rd_{MEAN}(\lambda)$ as the inputs, was sensitivity = 75%, specificity = 83.3%, and total correct classification = 79.3%.
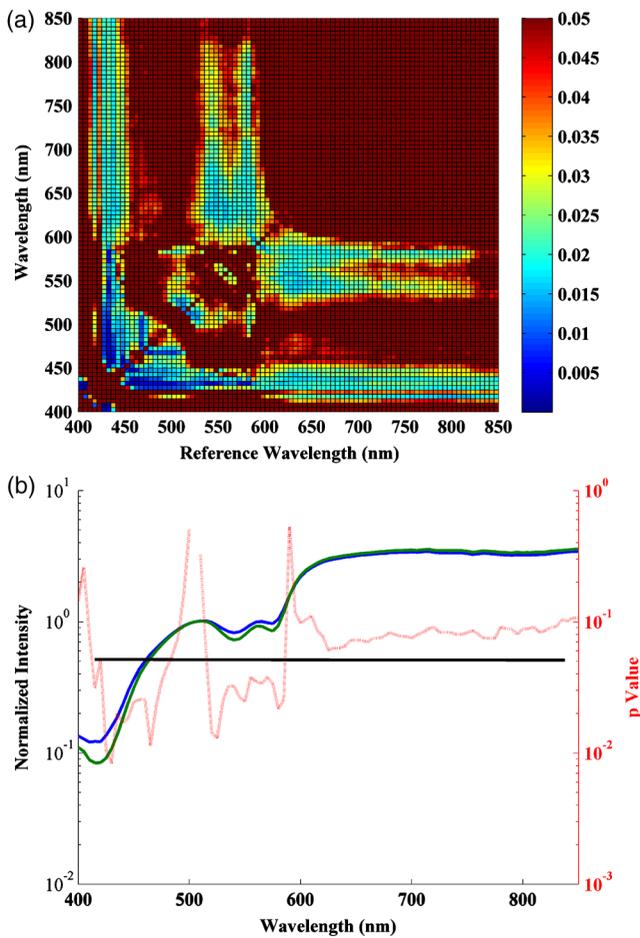
Fig. 4 (a) Surface plot of the *p* values from the mean comparison of $Rd(\lambda)/Rd(\lambda_{ref})$ between normal and epileptic brains. (b) Representative test results with reference wavelength $\lambda_{ref} = 505$ nm. The solid green line represents the mean $Rd(\lambda)/Rd(\lambda_{ref})$ of the normal brain group, and the solid blue line represents the mean $Rd(\lambda)/Rd(\lambda_{ref})$ of the epileptic brain group. Statistically significant differences (i.e., $p < 0.05$) are found between 425 and 460 nm and between 535 and 575 nm in this case.
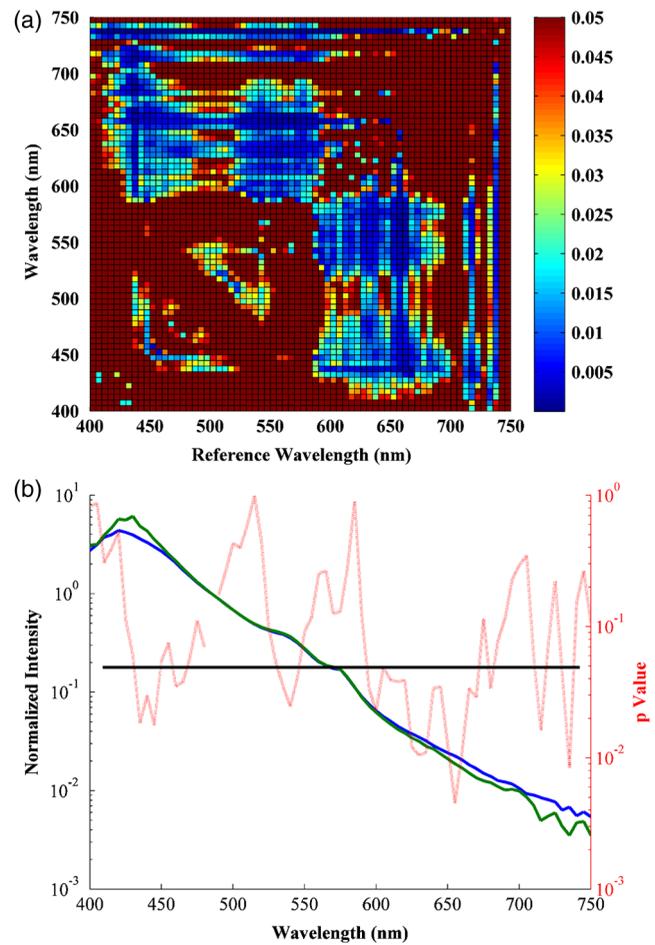

Fig. 5 (a) Surface plot of *p* values from the mean comparison of $[F(\lambda)/Rd(\lambda)]/[F(\lambda_{ref})/Rd(\lambda_{ref})]$ between normal and epileptic brains. (b) Representative test results with reference wavelength $\lambda_{ref} = 485$ nm. The solid green line represents the mean $[F(\lambda)/Rd(\lambda)]/[F(\lambda_{ref})/Rd(\lambda_{ref})]$ of the normal brain group, and the solid blue line represents the mean $[F(\lambda)/Rd(\lambda)]/[F(\lambda_{ref})/Rd(\lambda_{ref})]$ of the epileptic brain group. The statistically significant differences (i.e., $p < 0.05$) are found between 430 and 450 nm and between 625 and 660 nm in this case.

Table 3 Classification results of the discriminations based on LDA, using $Rd(\lambda)/Rd(\lambda_{ref})$ as the inputs.

λ_{ref} (nm)	Sensitivity (%)	Specificity (%)	Total correct classification (%)
445	75	86.7	81
455	75	80	77.6
460	75	83.3	79.3
500	78.6	90	84.5
505	**82.2**	**90**	**86.2**
535	78.6	86.7	82.8
550	78.6	86.7	82.8
605	78.6	86.7	82.8

The bold values represent the best results.

an epileptic brain. Again, the majority of these spectral features were located between $\lambda_{ref} = 400$ and $\lambda_{ref} = 600$ nm. Entering the identified spectral features, the classification results based on LDA yielded a sensitivity above 75% and a specificity above 80% (Table 4). Discrimination was optimized when λ_{ref} was 485 nm, where the overall accuracy of the discrimination algorithm was 96.6%.

4 Discussion

The *in vivo* study results demonstrate that *in vivo* static diffuse reflectance spectroscopy, as well as its combination with static fluorescence spectroscopy, can be used effectively to differentiate an epileptic brain (as defined by ECoG and histology) from a normal brain with a high degree of accuracy. The most effective discrimination algorithm is derived using the spectral features from $[F(\lambda)/Rd(\lambda)]/[F(485 \text{ nm}/Rd(485 \text{ nm})]$, where discrimination accuracy reaches 96.6%. This supports the concept of developing a new intraoperative guidance system, based on optical spectroscopy, to detect histopathological abnormalities associated with an epileptic brain in the operating room

Table 4 Classification results of the discriminations based on LDA, using $[F(\lambda)/Rd(\lambda)]/[F(\lambda_{\text{ref}})/Rd(\lambda_{\text{ref}})]$ as the inputs.

λ_{ref} (nm)	Sensitivity (%)	Specificity (%)	Total correct classification (%)
400	75.0	83.3	79.3
420	75.0	86.7	81.0
455	89.3	86.7	87.9
485	**92.9**	**100.0**	**96.6**
500	85.7	90.0	87.9
505	89.3	90.0	89.7
510	89.3	90.0	89.7
520	92.9	90.0	91.4

The bold values represent the best results.

and thereby provide additional information to aid in the demarcation of epileptic foci.

Using parametric and nonparametric statistical comparison methods, original $Rd(\lambda)$, $Rd_{\text{MEAN}}(\lambda)$, and $Rd(\lambda)/Rd(\lambda_{\text{ref}})$ between 400 and 600 nm were found to be significantly different in epileptic brains versus normal brains. Since diffuse reflectance spectra in this region are heavily influenced by hemoglobin absorption, this finding implies that certain static hemodynamic characteristics of the epileptic cortex, in particular hemoglobin concentration and hemoglobin oxygenation, are very different from that of a normal cortex. Previous studies have shown that hypometabolism and hypoperfusion are frequently observed in the area of an epileptic focus and its immediate surroundings in the brain of patients with partial seizures.[39–44] In addition, Stefanovic et al. pointed out that normal interictal neurovascular coupling is progressively compromised by sustained seizure attacks.[44] Schwartz suggested that the epileptic cortex generally receives inadequate cerebral blood flow.[45] However, alterations in resting state hemodynamics may not exist in all types of refractive epilepsy. It has been shown that the average resting metabolism and blood flow of the epileptic cortex are very similar to those of the normal cortex in patients with idiopathic generalized epilepsy.[46–48] Because of significant differences in the discharge characteristics of ictal versus interictal states, it has been suggested that the cerebral blood flow and cerebral metabolic rate of oxygen changes induced by interictal discharges may be far less noticeable than their ictal counterparts.[39,47,49] This implies that the changes in diffuse reflectance signals reported here are not necessarily associated with the presence of interictal discharges. The results of this study further suggest that histological abnormalities may be linked to changes in regional resting state hemodynamics. It is possible that histological abnormalities like cortical dysplasia modify the characteristics of astrocytic Ca^{2+} oscillations, which in turn alter astrocytic function regulating cerebral blood vessel diameters and hence regional hemodynamics.[50–54] More studies must be conducted to verify such conjectures.

Several studies have shown that the metabolic activities of any *in vivo* biological tissue, including the brain, may be monitored through the redox state of NAD(P)H and hence its

fluorescence.[27,28] Since the epileptic cortex is hypometabolic,[39–44] we hypothesized that fluorescence spectroscopy alone may be used to detect this characteristic of an epileptic brain. However, the results reported here do not support this hypothesis; no statistically significant differences were found between the fluorescence spectra from an epileptic brain and those from a normal brain. One possible explanation for this inefficiency is that NAD(P)H fluorescence signals measured from an *in vivo* brain are heavily modulated by brain absorption (i.e., hemoglobin concentration and hemoglobin oxygenation) and scattering properties. Under this condition, complex spectral processing techniques[55] would have to be used in conjunction with fluorescence spectroscopy to recover intrinsic NAD(P)H fluorescence quantity and hence detect the hypometabolic characteristic of the epileptic cortex.

The results of this study are promising but preliminary in nature. Several obstacles must be overcome before the clinical value of optical spectroscopy, namely fluorescence and diffuse reflectance spectroscopy, is clarified for demarcating epileptic foci and hence aiding epilepsy surgery. The most important challenge is the lack of a gold standard for defining an epileptic brain. While optical spectroscopy can indirectly detect histological abnormalities of an epileptic brain, it is not yet proven that these histological features provide better demarcation than ECoG. Furthermore, this study also revealed considerable discrepancies between the results of ECoG and those of histological study. On many occasions, the brain area classified as abnormal by ECoG was interpreted as histologically normal by our neuropathologist. This may be attributed to the fact that only small biopsy samples (i.e., less than 10 mm^3) were taken from the investigated sites within the resection zones for the purpose of accomodating the limited depth of investigation of the optical probe. Therefore, histopathological abnormalities present in the deeper layers of the cortex could be missed. Another possible explanation is that conventional histological methods cannot detect molecular alterations underlying the abnormal electrical activities of the epileptic cortex. Also, it is possible that the origin of interictal spikes may not be the same as that defined by ECoG due to electrical spreading. Finally, it will be challenging to establish a universal normal baseline for the diffuse reflectance and fluorescence spectra of a normal pediatric cortex, because the brain undergoes development and increases in size and weight significantly throughout childhood. These issues will be addressed in follow-up studies to be conducted by the current investigators, and their results will be presented in future publications.

5   Conclusions

The feasibility of using diffuse reflectance and fluorescence spectroscopy to aid epilepsy surgery in children was investigated. Static diffuse reflectance and fluorescence data were collected from the abnormal cortex, as defined by pathology and ECoG. Tissue discrimination algorithms with high sensitivity and specificity were produced using various spectral features. The success of this study warrants a future large-scale study to verify the potential role of optical spectroscopy in pediatric epilepsy surgery.

References

1. J. Williams and G. B. Sharp, *Pediatric Neuropsychology: Research, Theory, and Practice*, K. O. Yeates and H. G. Taylor, Eds., The Guilford Press, New York (2000).
2. P. Kwan and M. J. Brodie, "Early identification of refractory epilepsy," *N. Engl. J. Med.* **342**(5), 314–319 (2000).
3. A. T. Berg et al., "Early development of intractable epilepsy in children: a prospective study," *Neurology* **56**(11), 1445–1452 (2001).
4. J. H. Cross et al., "Proposed criteria for referral and evaluation of children for epilepsy surgery: recommendations of the subcommission for pediatric epilepsy surgery," *Epilepsia* **47**(6), 952–959 (2006).
5. J. Engel Jr., "Surgery for seizures," *N. Engl. J. Med.* **334**(10), 647–652 (1996).
6. A. S. Harvey et al., "Defining the spectrum of international practice in pediatric epilepsy surgery patients," *Epilepsia* **49**(1), 146–155 (2008).
7. K. Chapman et al., "Seizure outcome after epilepsy surgery in patients with normal preoperative MRI," *J. Neurol. Neurosurg Psychiatry* **76**(5), 710–713 (2005).
8. M. Hemb et al., "Improved outcomes in pediatric epilepsy surgery: the UCLA experience, 1986–2008," *Neurology* **74**(22), 1768–1775 (2010).
9. D. Zumsteg and H. G. Wieser, "Presurgical evaluation: current role of invasive EEG," *Epilepsia* **41**(Suppl 3), S55–S60 (2000).
10. F. Sperli et al., "EEG source imaging in pediatric epilepsy surgery: a new perspective in presurgical workup," *Epilepsia* **47**(6) 981–990 (2006).
11. D. W. Roberts et al., "Intraoperative brain shift and deformation: a quantitative analysis of cortical displacement in 28 cases," *Neurosurgery* **43**(4), 749–758 (1998).
12. C. Nimsky et al., "Intraoperative compensation for brain shift," *Surg. Neurol.* **56**(6), 357–364 (2001).
13. C. Nimsky et al., "Quantification of, visualization of, and compensation for brain shift using intraoperative magnetic resonance imaging," *Neurosurgery* **47**(5), 1070–1079 (2000).
14. S. Ding et al., "Estimation of intra-operative brain shift using a tracked laser range scanner," in *29th Ann. Int. Conf. Proc. IEEE Eng. Med. Biol. Soc.*, pp. 848–851, IEEE (2007).
15. E. Asano et al., "Role of subdural electrocorticography in prediction of long-term seizure outcome in epilepsy surgery," *Brain* **132**(Pt 4), 1038–1047 (2009).
16. V. Jay and L. E. Becker, "Surgical pathology of epilepsy: a review," *Pediatr. Pathol.* **14**(4), 731–750 (1994).
17. J. M. Paolicchi et al., "Predictors of outcome in pediatric epilepsy surgery," *Neurology* **54**(3), 642–647 (2000).
18. R. Richards-Kortum and E. Sevick-Muraca, "Quantitative optical spectroscopy for tissue diagnosis," *Annu. Rev. Phys. Chem.* **47**(1), 555–606 (1996).
19. K. Sokolov, M. Follen, and R. Richards-Kortum, "Optical spectroscopy for detection of neoplasia," *Curr. Opin. Chem. Biol.* **6**(5), 651–658 (2002).
20. Z. Huang et al., "Near-infrared Raman spectroscopy for optical diagnosis of lung cancer," *Int. J. Cancer* **107**(6), 1047–1052 (2003).
21. W.-C. Lin et al., "*In vivo* brain tumor demarcation using optical spectroscopy," *Photochem. Photobiol.* **73**(4), 396–402 (2001).
22. A. Gillenwater et al., "Noninvasive diagnosis of oral neoplasia based on fluorescence spectroscopy and native tissue autofluorescence," *Arch. Otolaryngol. Head. Neck. Surg.* **124**(11), 1251–1258 (1998).
23. J. R. Mourant et al., "Spectroscopic diagnosis of bladder cancer with elastic light scattering," *Lasers Surg. Med.* **17**(4), 350–357 (1995).
24. G. M. Palmer et al., "Comparison of multiexcitation fluorescence and diffuse reflectance spectroscopy for the diagnosis of breast cancer," *IEEE Trans. Biomed. Eng.* **50**(11), 1233–1242 (2003).
25. G. Zonios et al., "Diffuse reflectance spectroscopy of human adenomatous colon polyps *in vivo*," *Appl. Opt.* **38**(31), 6628–6637 (1999).
26. I. J. Bigio and J. R. Mourant, "Ultraviolet and visible spectroscopies for tissue diagnostics: fluorescence spectroscopy and elastic-scattering spectroscopy," *Phys. Med. Biol.* **42**(5), 803–814 (1997).
27. G. A. Wagnieres, W. M. Star, and B. C. Wilson, "*In vivo* fluorescence spectroscopy and imaging for oncological applications," *Photochem. Photobiol.* **68**(5), 603–632 (1998).
28. A. Mayevsky and B. Chance, "Oxidation-reduction states of NADH *in vivo*: from animals to clinical use," *Mitochondrion* **7**(5), 330–339 (2007).
29. D. A. Boas et al., "The accuracy of near infrared spectroscopy and imaging during focal changes in cerebral hemodynamics," *Neuroimage* **13**(1), 76–90 (2001).
30. A. Villringer et al., "Near infrared spectroscopy (NIRS): a new tool to study hemodynamic changes during activation of brain function in human adults," *Neurosci. Lett.* **154**(1–2), 101–104 (1993).
31. A. Mayevsky and G. G. Rogatsky, "Mitochondrial function *in vivo* evaluated by NADH fluorescence: from animal models to human studies," *Am. J. Physiol. Cell. Physiol.* **292**(2), C615–C640 (2007).
32. W.-C. Lin et al., "Diffuse reflectance spectroscopy for *in vivo* pediatric brain tumor detection," *J. Biomed. Opt.* **15**(6), 061709 (2010).
33. S. Bhatia et al., "The role of optical spectroscopy in epilepsy surgery in children," *Neurosurg. Focus* **25**(3), E24 (2008).
34. S. Oh et al., "*In vivo* optical properties of cortical tubers in children with tuberous sclerosis complex (TSC): a preliminary investigation," *Epilepsia* **52**(9), 1699–1704 (2011).
35. M. M. Haglund and D. W. Hochman, "Optical imaging of epileptiform activity in human neocortex," *Epilepsia* **45**(Suppl 4), 43–47 (2004).
36. M. Zhao et al., "Focal increases in perfusion and decreases in hemoglobin oxygenation precede seizure onset in spontaneous human epilepsy," *Epilepsia* **48**(11), 2059–2067 (2007).
37. M. M. Haglund, "Optical imaging of visual cortex epileptic foci and propagation pathways," *Epilepsia* **53**(Suppl 1), 87–97 (2012).
38. W.-C. Lin et al., "Brain tumor demarcation using optical spectroscopy; an *in vitro* study," *J. Biomed. Opt.* **5**(2), 214–220 (2000).
39. J. Engel Jr. et al., "Interictal cerebral glucose metabolism in partial epilepsy and its relation to EEG changes," *Ann. Neurol.* **12**(6), 510–517 (1982).
40. G. Franck et al., "Regional cerebral blood flow and metabolic rates in human focal epilepsy and status epilepticus," *Adv. Neurol.* **44**, 935–948 (1986).
41. S. K. Kim et al., "Diagnostic performance of [18F]FDG-PET and ictal [99mTc]-HMPAO SPECT in occipital lobe epilepsy," *Epilepsia* **42**(12), 1531–1540 (2001).
42. D. E. Kuhl et al., "Epileptic patterns of local cerebral metabolism and perfusion in humans determined by emission computed tomography of 18FDG and 13NH3," *Ann. Neurol.* **8**(4), 348–360 (1980).
43. B. I. Lee et al., "Single photon emission computed tomography (SPECT) brain imaging using N,N,N'-trimethyl-N'-(2-hydroxy-3-methyl-5-123I-iodobenzyl)-1,3-propanediamine 2 HCl (HIPDM): intractable complex partial seizures," *Neurology* **36**(11), 1471–1477 (1986).
44. B. Stefanovic et al., "Hemodynamic and metabolic responses to activation, deactivation and epileptic discharges," *Neuroimage* **28**(1), 205–215 (2005).
45. T. H. Schwartz, "Neurovascular coupling and epilepsy: hemodynamic markers for localizing and predicting seizure onset," *Epilepsy Curr.* **7**(4), 91–94 (2007).
46. J. S. Duncan, "Imaging and epilepsy," *Brain* **120**(2), 339–377 (1997).
47. W. H. Theodore et al., "Positron emission tomography in generalized seizures," *Neurology* **35**(5), 684–690 (1985).
48. L. O. Kapucu et al., "Brain single photon emission computed tomographic evaluation of patients with childhood absence epilepsy," *J. Child. Neurol.* **18**(8), 542–548 (2003).
49. M. C. Prevett et al., "Demonstration of thalamic activation during typical absence seizures using H2(15)O and PET," *Neurology* **45**(7), 1396–1402 (1995).
50. G. R. Gordon, S. J. Mulligan, and B. A. MacVicar, "Astrocyte control of the cerebrovasculature," *Glia* **55**(12), 1214–1221 (2007).
51. G. Balazsi, A. H. Cornell-Bell, and F. Moss, "Increased phase synchronization of spontaneous calcium oscillations in epileptic human versus normal rat astrocyte cultures," *Chaos.* **13**(2), 515–518 (2003).
52. S. Ding et al., "Enhanced astrocytic Ca2+ signals contribute to neuronal excitotoxicity after status epilepticus," *J. Neurosci.* **27**(40), 10674–10684 (2007).
53. H. Hirase et al., "Calcium dynamics of cortical astrocytic networks *in vivo*," *PLoS Biol.* **2**(4), E96 (2004).
54. A. Tashiro, J. Goldberg, and R. Yuste, "Calcium oscillations in neocortical astrocytes under epileptiform conditions," *J. Neurobiol.* **50**(1), 45–55 (2002).
55. M. G. Mueller et al., "Intrinsic fluorescence spectroscopy in turbid media: disentangling effects of scattering and absorption," *Appl. Opt.* **40**(25), 4633–4646 (2001).